SOFT ROBOTS

Shape morphing mechanical metamaterials through reversible plasticity

Dohgyu Hwang[1,2]†, Edward J. Barron III[1,2]†, A. B. M. Tahidul Haque[2], Michael D. Bartlett[1,2]*

Biological organisms such as the octopus can reconfigure their shape and properties to perform diverse tasks. However, soft machines struggle to achieve complex configurations, morph into shape to support loads, and go between multiple states reversibly. Here, we introduce a multifunctional shape-morphing material with reversible and rapid polymorphic reconfigurability. We couple elastomeric kirigami with an unconventional reversible plasticity mechanism in metal alloys to rapidly (<0.1 seconds) morph flat sheets into complex, load-bearing shapes, with reversibility and self-healing through phase change. This kirigami composite overcomes trade-offs in deformability and load-bearing capacity and eliminates power requirements to sustain reconfigured shapes. We demonstrate this material through integration with onboard control, motors, and power to create a soft robotic morphing drone, which autonomously transforms from a ground to air vehicle and an underwater morphing machine, which can be reversibly deployed to collect cargo.

INTRODUCTION

Shape-morphing materials with tunable rigidity are key components for emerging technologies, ranging from stretchable electronics and soft robotics to reconfigurable structures and multimodal vehicles (*1*–*4*). Key to these systems is the ability to occupy complex configurations, to maintain shape without consuming power, and to go between multiple states reversibly. However, such attributes are uncommon in a single material system. One promising approach to create morphing systems is to use initially flat sheets that contain designed geometric features. For example, by incorporating cuts (kirigami) or folds (origami) into materials, prescribed three-dimensional (3D) output shapes can be obtained under deformation (*5*–*8*). This class of materials, often referred to as mechanical metamaterials, allows for a high degree of freedom and high extensibility (*9*, *10*). These systems are particularly appealing for shape morphing because of the energetically favorable bending modes driven by the slender structures in kirigami networks, compared with continuous membranes whose deformation is dominated by stretching modes that can cause structural collapse (*11*). However, the reconfigurability and reversibility of such systems can be limited, because the structures are often bistable (*12*, *13*), require applied loads to maintain configurations due to elastic restoring forces (*14*), or use permanent deformation to change shapes (*15*, *16*). Bistable metamaterials can successfully go between different stable states, but achievable shapes are often dictated prefabrication by prescribed designs and specific loading conditions, which can limit field reconfigurability or multifunctionality during use (*17*, *18*). Furthermore, the intrinsic trade-off between load-bearing capacity and high deformability in homogeneous sheets is limiting for soft matter engineering applications that require notable shape change and structural strength (*19*).

Another approach to creating morphing systems is to control material properties across a sheet. This is often achieved by tuning deformations through heterogeneous material stiffness or placing responsive materials at prescribed locations (*20*–*22*). For example, stiffness gradients or swelling regions can allow for expansion at different locations for prescribed, reversible shapes. This can be driven through stimuli such as differential growth or swelling (*23*, *24*), pneumatics (*22*, *25*), heat (*26*), electric fields (*27*), and magnetic fields (*28*). However, morphing with these mechanisms cannot be obtained without constantly applied stimuli or energy inputs (e.g., pressure, specific solvent/temperatures, and magnetic field), because the reconfigured shape is maintained by a specific condition or applied field. One way to overcome limited shape reconfigurability is to leverage variable stiffness materials, such as those driven through phase change, or shape memory materials (*4*, *29*–*34*). However, continuous membrane geometries can limit shape fixity, and reconfiguration through melting and subsequent cooling to maintain different configurations is intrinsically slow because of thermal diffusion (*35*).

Here, we introduce shape- and rigidity-morphing materials with reversible and rapid polymorphic 3D reconfigurability and programmable stiffness (Fig. 1). The material rapidly morphs (<0.1 s) into load-bearing configurations yet reconfigures and self-heals through a phase transition for shape and stiffness reconfigurability. To achieve this, we created a kirigami composite metamaterial sheet that synergistically combines shape morphing by nonlinear deformations of elastomeric kirigami architectures, shape fixing by nonlinear material response through plasticity and phase change of an embedded low–melting point alloy (LMPA), and reversibility with an integrated heater to trigger a phase change in the LMPA to elastically recover plastic deformation.

The elastomeric kirigami architecture undergoes extreme deformations, achieves complex shapes, and displays nonlinear force-extension characteristics, which allows for minimal restoring forces at high extensibility, enabling high shape retention during shape fixing in different configurations. The LMPA (Field's metal) displays material nonlinearities for shape morphing, which we introduce through an unconventional reversible plasticity mechanism. Although plasticity (a nonreversible change of shape in response to applied force) is typically associated with material failure, we now use this mechanism to introduce advanced functionality: the rapid reconfiguration of shapes in soft materials that become instantly load bearing. The

[1]Macromolecules Innovation Institute, Virginia Tech, Blacksburg, VA 24061, USA. [2]Department of Mechanical Engineering, Soft Materials and Structures Lab, Virginia Tech, Blacksburg, VA 24061, USA.
*Corresponding author. Email: mbartlett@vt.edu
†These authors contributed equally to this work.

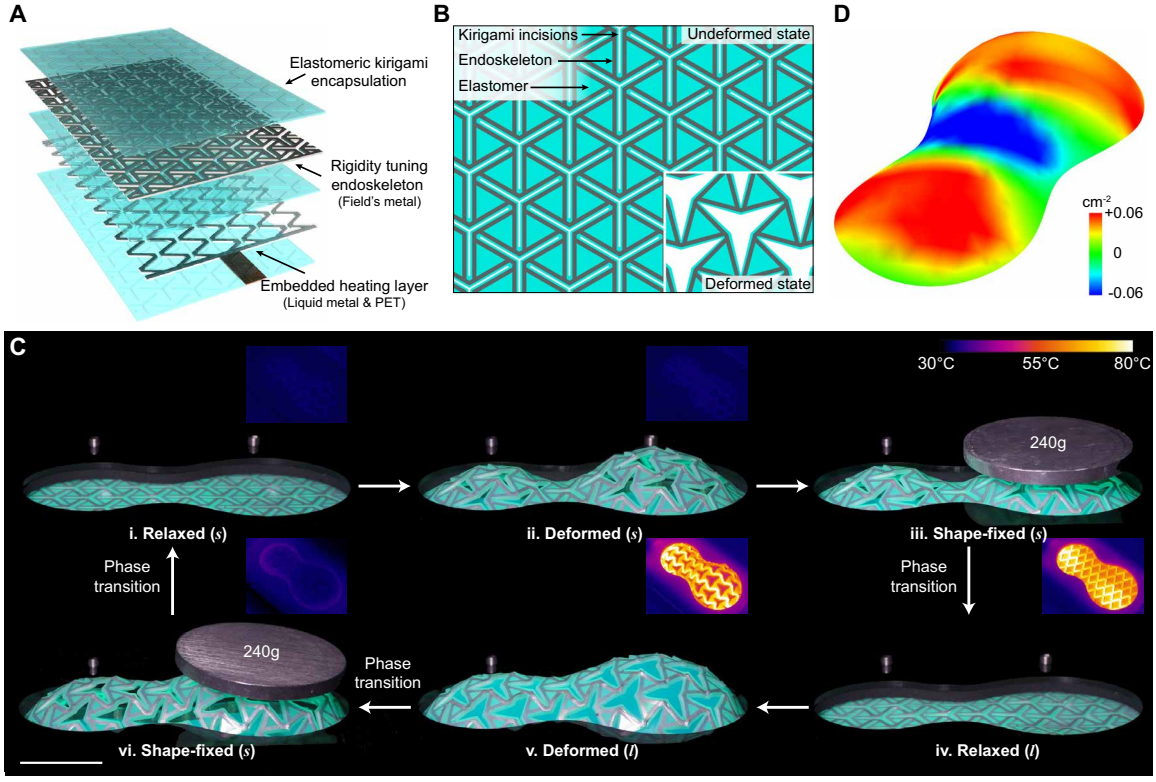

Fig. 1. Multimaterial kirigami composite with instantaneous complex shape fixing and reversibility. (**A**) Schematic showing the layers of a kirigami-inspired multilayered composite. (**B**) A top-down schematic showing the kirigami incisions, endoskeleton, and elastomer in an undeformed state with the deformed state in the inset. (**C**) Image sequence showing the composite morphing into the programmed shape of an inflating elastomeric membrane underneath and supporting 240 g in the reconfigured state after the membrane is deflated. By activating embedded heaters [inset shows infrared (IR) images], the morphed composite undergoes a phase change and returns to the flat initial state and can then be actuated repeatedly. Scale bar, 50 mm. (**D**) Gaussian curvature map of the deployed kirigami composite showing the complex shape.

LMPA intrinsically deforms plastically at low strains, which we leverage to immediately morph the material into load-bearing shapes (<0.1 s). Mechanical deformation induces plasticity that sustains the shape without any electrical energy consumption or time limitations due to mass or thermal transport. Yet, the shape is reversible by using the embedded heaters to melt the LMPA, which then allows the elastomeric kirigami to elastically reverse the plasticity and enable reconfigurability and self-healing over numerous cycles. By patterning the elastomer and embedded LMPA with kirigami patterns, complex shapes are achievable and can display combinations of negative, zero, and positive Gaussian curvature. Thus, by combining kirigami structures, LMPA, and embedded heaters, our multimaterial system displays extreme deformations and reversible plasticity. This approach achieves rapid shape fixing into complex configurations and maintains reversibility and load-bearing capacity. This approach overcomes limitations in morphing material systems and trade-offs between extensibility and load-bearing capacity in reconfigurable soft systems. These materials are integrated with onboard power, control, motors, and embedded heaters to create a functional morphing drone with multiple remotely controlled locomotion modes enabled by an autonomous morphing from a ground to air vehicle configuration. We further show a morphing underwater machine that can be reversibly deployed to collect cargo through integrated water propulsion and buoyancy control.

RESULTS

Morphing composite design

The composite consists of a rigidity tuning endoskeleton made of an LMPA, an embedded heating layer, and elastomeric kirigami encapsulation (Fig. 1A). The LMPA is Field's metal—which is a eutectic alloy of bismuth, indium, and tin—and transitions from a high elastic modulus (>3 GPa) solid to a flowable liquid at relatively low melting temperatures (melting point of 62°C) (*29*). The sample was fabricated by first creating the endoskeleton through a vacuum-assisted replica molding process that enabled arbitrary continuous geometries. This design flexibility can create common kirigami designs such as uniaxial, biaxial, and triaxial cut patterns (see fig. S1). The endoskeleton and heating layers were then embedded in elastomer, and kirigami incisions were laser-cut throughout the sample to define the kirigami geometry (Fig. 1B). To demonstrate the rapid shape-morphing capability and reversibility, a relaxed triaxial kirigami composite in the solid state was deformed through an inflated pneumatic membrane (Fig. 1C). This film rapidly morphed into a doubly curved surface with complex curvature, as demonstrated by a curvature map showing the positive and negative Gaussian curvatures (Fig. 1D). Upon deflating the underlying membrane, the free-standing kirigami film was reconfigured into the programmed shape through plasticity. Because of the rigidity of the solid endoskeleton, the structure immediately achieved load-bearing capacity

and supported a disk-shaped weight (240 g). However, by electrically activating the embedded heater through Joule heating, the endoskeleton underwent a phase transition to a liquid phase, and the elasticity of the elastomer returned the structure into a relaxed, liquid state. This phase change, coupled with the elasticity of the elastomer, enables reversible plasticity. The structure can be morphed in the liquid state to become highly compliant. By holding the deformed state and undergoing a phase transition back to a solid state, the kirigami film becomes rigid to regain a load-bearing configuration. This process can be repeated by activating the heater to return the film to a relaxed, solid state.

Morphing composite mechanical analysis

The kirigami composite was mechanically analyzed under uniaxial loading for different endoskeleton states and geometries of the LMPA endoskeletons (Fig. 2A). Figure 2B shows representative load P versus applied strain ε_{appl} curves for kirigami composites in either a solid state, a liquid state, or elastomer without an LMPA endoskeleton. Each specimen was cyclically loaded three times to 100% strain and then returned to zero strain, with the unloading step performed in the liquid endoskeleton state. The solid-state composite is shown to be rigid (effective stiffness, K_{eff} = 8480 ± 770 N/m) in the initial loading ($\varepsilon_{appl} \leq 10\%$); however, once localized plastic deformation was observed, the load-displacement response became nonlinear. At this point, substantial softening and a slight negative stiffness were observed, where the structure extended with minimal additional strain energy. This load plateau after initial loading is critical because this allows for high degrees of shape reconfigurability as discussed below. In contrast, the liquid-state composite exhibited a soft response with a negligible effective stiffness (K_{eff} = 65 ± 10 N/m), which is ~130 times softer than the solid state (Fig. 2D) and softer than the elastomeric kirigami alone.

We determined the underlying elastoplastic morphing mechanism of the endoskeleton in the solid state using finite element analysis (FEA). We followed the multilayered kirigami composite of Fig. 2A to develop the layered composite section for the FE model. The LMPA was simulated with elastoplastic material behavior, and the elastomeric layers were modeled by a hyperelastic formulation. The Materials and Methods section for FEA describes materials and elements in more detail. The FEA accurately captures the experimental load-strain characteristics for the solid-phase kirigami composite in Fig. 2B. Furthermore, the FEA gives insight into the plastic deformation process at a material level. In Fig. 2C, FEA results illustrate the plastic hinge formation at the joints of kirigami beams at different stages of global strain ε_{appl} = 0, 10, and 100%. The kirigami joints remained primarily elastic until reaching ε_{appl} = 10%, where most of the plastic hinges were formed. Thereafter, the plastic zone intensified around kirigami joints, and the kirigami structure deformed without any marked resistance to the applied strain ε_{appl}. Stress concentrations are common in kirigami structures near the

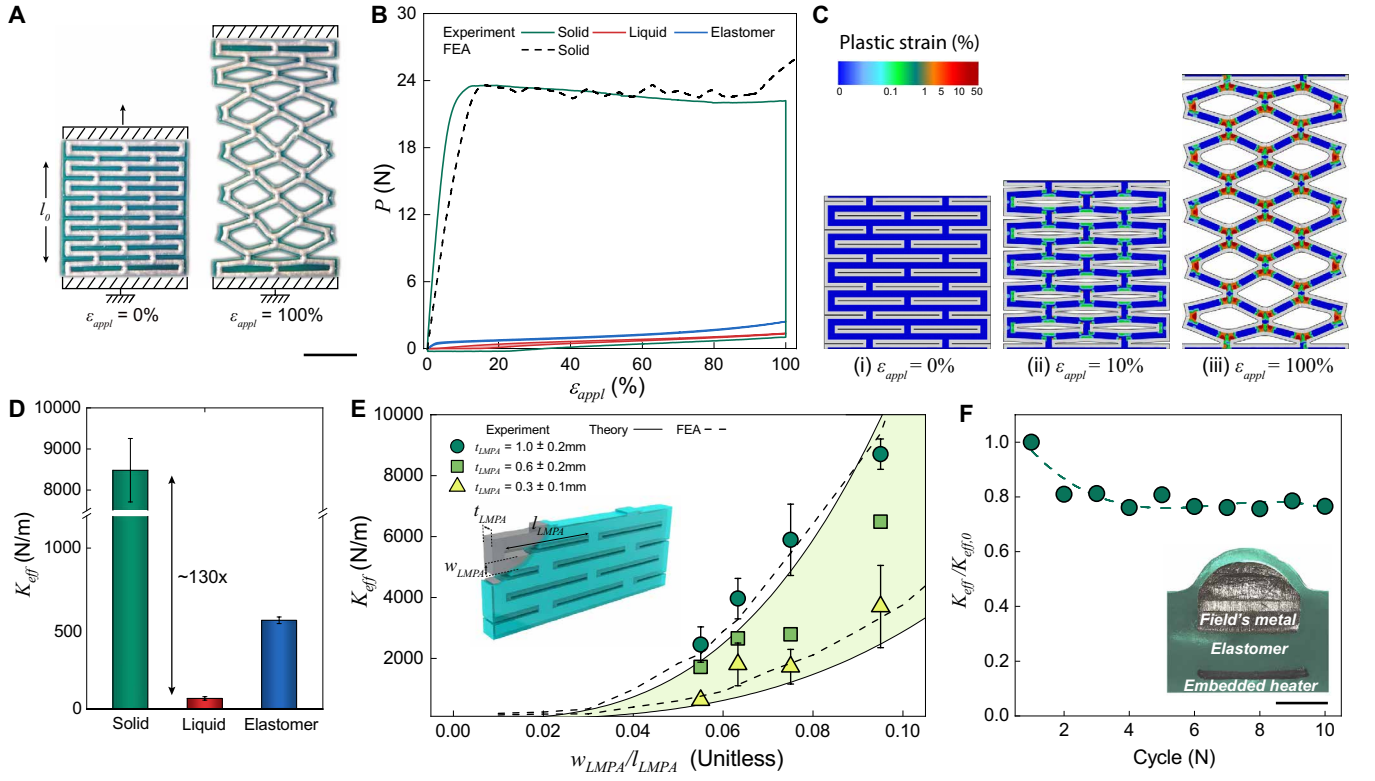

Fig. 2. Mechanical performance of kirigami composites with uniaxial endoskeleton structures. (**A**) Kirigami composite at 0 and 100% strain. Scale bar, 20 mm. (**B**) Load versus applied tensile strain for different kirigami composites (l_{LMPA} = 20 mm, width w_{LMPA} = 1.9 mm, and thickness t_{LMPA} = 1000 μm). (**C**) FEA results showing the development of plastic hinges at different applied strains. (**D**) Kirigami composite stiffness for different endoskeleton states. Error bars represent the SD for n = 10. (**E**) Effective stiffness versus kirigami beam geometry w_{LMPA}/l_{LMPA} for kirigami composites with 12 different endoskeleton geometries. Inset: Composite schematic showing geometric parameters. Error bars represent the SD for n = 3. (**F**) Normalized stiffness as a function of the number of cycles for an LMPA-embedded kirigami composite. Inset: a cross section of the composite. Scale bar, 1 mm.

vicinity of the cut, which enhances the generation of plasticity in these regions (*36*). This local plastic deformation contributes to the soft structural response of the solid-state kirigami between ε_{appl} = 10 and 100% in Fig. 2B and allows for the composite to be morphed into different stable configurations.

The effective stiffness of the structure (K_{eff}) can also be tuned by controlling the kirigami geometry, where the stiffness K_{eff} can be calculated as

$$K_{eff} = \beta \frac{E w^3 t}{l^3} \quad (1)$$

where β depends on boundary conditions and system size, and t, w, and l are beam thickness, width, and length, respectively (*10*). We investigated various compositions of LMPA beams—such as length (l_{LMPA} = 20 and 30 mm), width (w_{LMPA} = 1.1, 1.5, and 1.9 mm), and thickness (t_{LMPA} ranging from 300 to 1000 μm)—with constant encapsulating layer geometry. In Fig. 2E, the upper line predicts stiffness of kirigami structures that include ~1-mm-thick endoskeletons with varying slenderness, and the lower line predicts that with ~0.3-mm-thick endoskeletons, with the shaded region indicating intermediate thickness and showing the large tunability through kirigami structure. The experimental data are well captured by the analytical solution and numerical analyses. The composite is also robust under cyclic loading (Fig. 2F). Here, the kirigami composite was deformed in the solid state to 100% strain, where after the first cycle the rigidity was stable for the remaining cycles (10 cycles were run). During this process, no fracture in the endoskeleton was observed. Robustness was further investigated by intentionally breaking the endoskeleton at multiple points, melting the composite endoskeleton, and then resolidifying at room temperature to heal the structure. The self-healing efficiency was then quantified by measuring the stiffness for 10 fracture/healing cycles. The stiffness of the healed sample was consistent with the pristine sample and showed no degradation over the 10 cycles, demonstrating excellent healing efficiency (fig. S2). Critical to this behavior is the overpressurization of the LMPA during fabrication (see figs. S3 to S5). This enables the material to flow back in contact and resolidify into a monolithic structure.

We quantify the shape-fixing capability of the kirigami composite through uniaxial cyclic experiments (Fig. 3A). Here, we apply strains of ε_{appl} = 10 to 50% and then unload under quasi-static conditions, until the load drops to zero (loading and unloading rate of 1 mm/s and 0.01 mm/s, respectively). The strain at zero load is the plastic strain (ε_p) and represents the amount of deformation that remains after morphing. We define the shape-fixity ratio R_f as

$$R_f = \frac{\varepsilon_p}{\varepsilon_{appl}} \quad (2)$$

We evaluate R_f as a function of ε_{appl} for two kirigami films with endoskeletons in the solid state (the stiffest and least stiff from Fig. 2E), an endoskeleton loaded in the liquid state and solidified at ε_{appl}, and a kirigami elastomer control without an endoskeleton (Fig. 3B). When the elastomer control (endoskeleton-free material) is deformed, nearly no shape retention occurs regardless of ε_{appl} because of the elastomer elasticity that restores the structure to the undeformed state. For the smallest stiffness solid endoskeleton, we observe 10% < R_f < 30%, where the low values of R_f are attributed to the restoring force of the elastomeric layers, which dominates over the endoskeleton. In contrast, the sample with the largest stiffness shows R_f ~ 30% for small ε_{appl} (2.5%) and reaches R_f ~ 85% for larger ε_{appl} (50%). Recall from Fig. 2B that the development of full plasticity in the kirigami endoskeleton requires ε_{appl} > 10%. Therefore, modest R_f for low ε_{appl} is attributed to a low degree of plastic deformation in the kirigami endoskeleton. A high shape-fixity ratio (≈100%) can be obtained by loading the sample at $T > T_m$ and holding it until the LMPA solidifies (see data points for Loaded in liquid in Fig. 3B). However, in this case, heating and cooling are required, and the morphing process can take minutes (*35*). In contrast, when loaded in the solid state, the material is instantaneously load bearing and does not require electrical energy input to maintain its reconfigured shape. We also varied the unloading rate to determine the time dependence of shape fixity for ε_{appl} = 50% and found that when varying the unloading rate by over two orders of magnitude (from 0.005 to 1 mm/s), R_f varies by less than 7% (see figs. S6 and S7) and is always higher than 83%.

Shape fixing

Kirigami architectures and material plasticity enable very rapid, large dynamic reconfigurability and stable shape fixity without a continuous input of energy. To demonstrate the rapid shape-fixing behavior, we created a kirigami composite with a spiral cut pattern and then impacted a metal ball (130 g) into the center of the composite (Fig. 3C). Upon impact of the metal ball, extreme deformation occurred in ~70 ms by dissipating the kinetic energy through large plastic deformation of the kirigami composite (movie S1). After removal of the metal ball and inversion of the structure, the deformed shape was maintained with an excellent shape fixity (R_f ~ 100%). The embedded heater was then activated to melt the LMPA endoskeleton, which allowed the elastomer to elastically reverse the plasticity and transformed the structure back to its initial configuration. This demonstrated the ability to achieve substantial deformation and shape fixing at rapid time scales through plasticity coupled with the ability to restore the initial configuration through heating and elastic recovery. To further demonstrate the shape-morphing capability of the kirigami composite, a single kirigami composite sheet with triangular cut patterns was morphed into various objects that exhibited positive (a spherical orange), zero (a cylindrical cucumber), and mixed Gaussian curvature (bottom of a bell pepper) shapes (Fig. 3D). The same sheet was reconfigured through heating to conform to the three different objects, demonstrating reversibility. The triaxial pattern enables planar expansions due to negative Poisson's ratio, ensuring good replication of the different complex shapes in three dimensions. This is characteristic of the nonlinear structural response of the system, where localized rotations or bending enables a minimal rise in force with increasing deformation. This low restoring force allows for shape-fixing capabilities in different complex configurations.

Morphing drone

Morphing materials that can support load and reconfigure shape without continuous energy input can enable highly adaptable and mobile machines. To demonstrate these enabling characteristics, the kirigami composite was used as a reconfigurable body to create a multifunctional, bimodal morphing soft robotic drone (Fig. 4, A and B). The kirigami-drone body consists of LMPA endoskeletons embedded in an elastomer to provide shape morphing and an embedded heating layer to enable phase transition of the endoskeleton. By integrating onboard power, control, antennas, and motors,

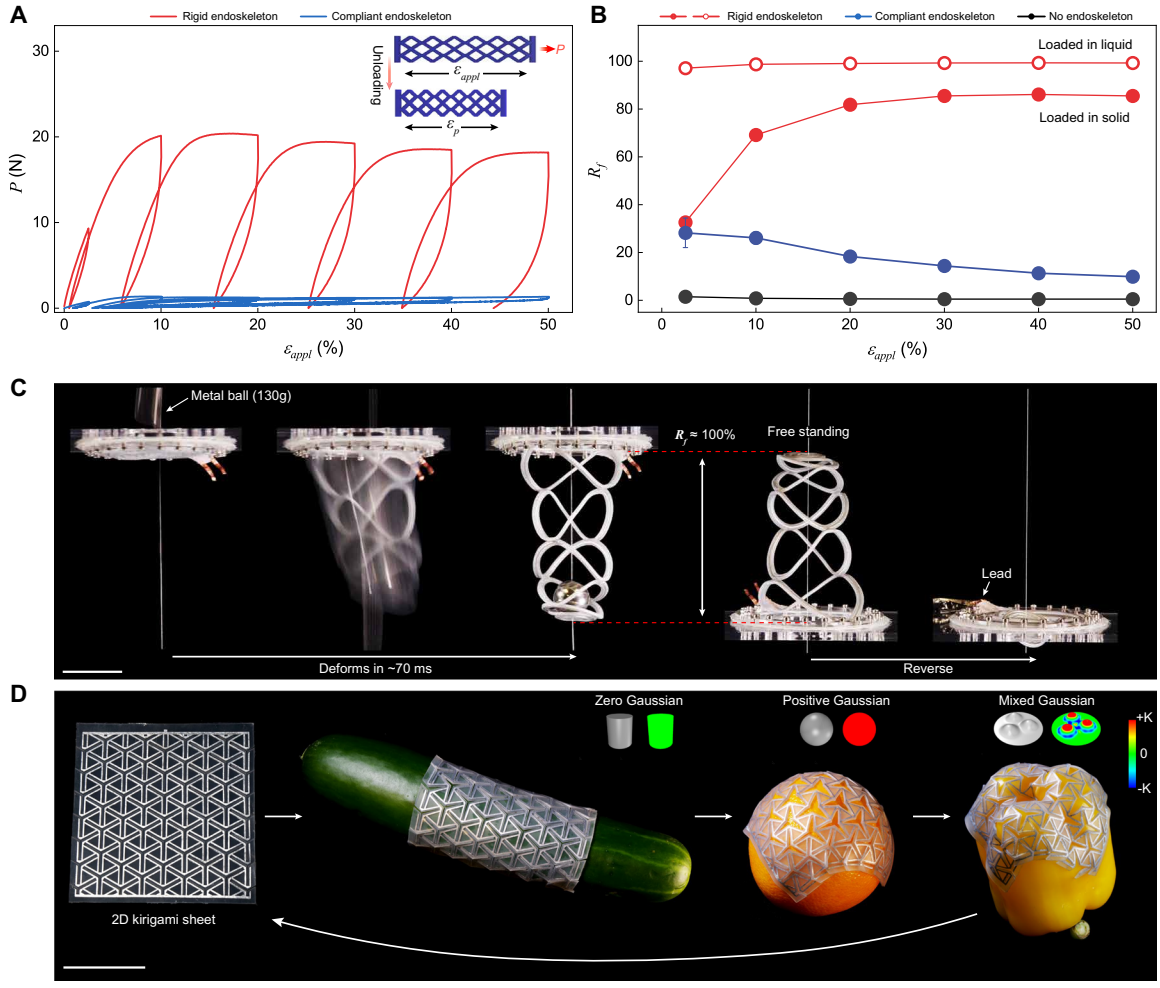

Fig. 3. Shape fixing at rapid time scales with complex shapes. (**A**) Load versus strain shape-fixing curves for two specimens with different kirigami stiffness and a sample without an endoskeleton. The inset presents a schematic of the measurement of a shape-fixity ratio (R_f). (**B**) Shape-fixity ratio R_f as a function of ε_{appl} from (A). Error bars represent the SD for $n = 3$. (**C**) A kirigami composite undergoes substantial out-of-plane deformation through the impact of a metal ball (movie S1), which causes rapid reconfiguration and shape fixing into the deformed shape in ~70 ms. The second to last image shows the structure inverted against gravity where it maintains the reconfigured shape, and the last image shows reversibility of the shape through activation of the embedded heater. Scale bar, 50 mm. (**D**) Photographs of a triaxial kirigami composite that morphs onto objects with complex curvatures reversibly. Insets show the representative Gaussian curvature of the objects. Scale bar, 50 mm.

the drone can be remotely driven in state 1 on the ground, autonomously morphed from a ground to air vehicle configuration, and then be flown in state 2 (Fig. 4C and movie S2). The embedded heater was localized at specific morphing points to enable the autonomous transformation from an upright driving state to the flat flying state (Fig. 4D). The shape transformation was initiated upon contact between copper wires on the drone and liquid metal layers deposited on a power transfer station (see Materials and Methods), which enabled transformation to occur with no external intervention. To measure the power for Joule heating, we normalized the power input by the interfacial area between the liquid metal channels and LMPA regions, and the value was measured to be 9.3 mW/mm^2. By going beyond manual reconfiguration or morphing demonstrations that lack integration of functional components, our morphing material–based drone achieves locomotion in multiple distinct configurations. The load-bearing capacity coupled with the ability to markedly transform configurations is critical to the locomotion modes and highlights the potential of our morphing kirigami composites to enable future applications in multifunctional systems for reconfigurable robotics and electronics.

Morphing and deployable underwater machine

The morphing kirigami composites presented here rapidly and reversibly morph into complex, load-bearing geometries without the need for continuous energy input. This combination of properties is enabling for deployable robots, which must exist in a slim, easily transportable form factor before being deployed to perform tasks. Morphing mechanisms can allow underwater machines to achieve advanced functions and deploy from a packed state (*37*, *38*). Different approaches to create underwater morphing robots have been shown; however, morphing has been predominantly used for locomotion (*38*–*41*). Creating a reversibly deployable machine with locomotion and sufficient mechanical stability to perform functions and practically interact with the environment remains a challenge (*42*–*45*). Motivated by this, we use kirigami composites to develop a deployable underwater machine capable of starting in a flat,

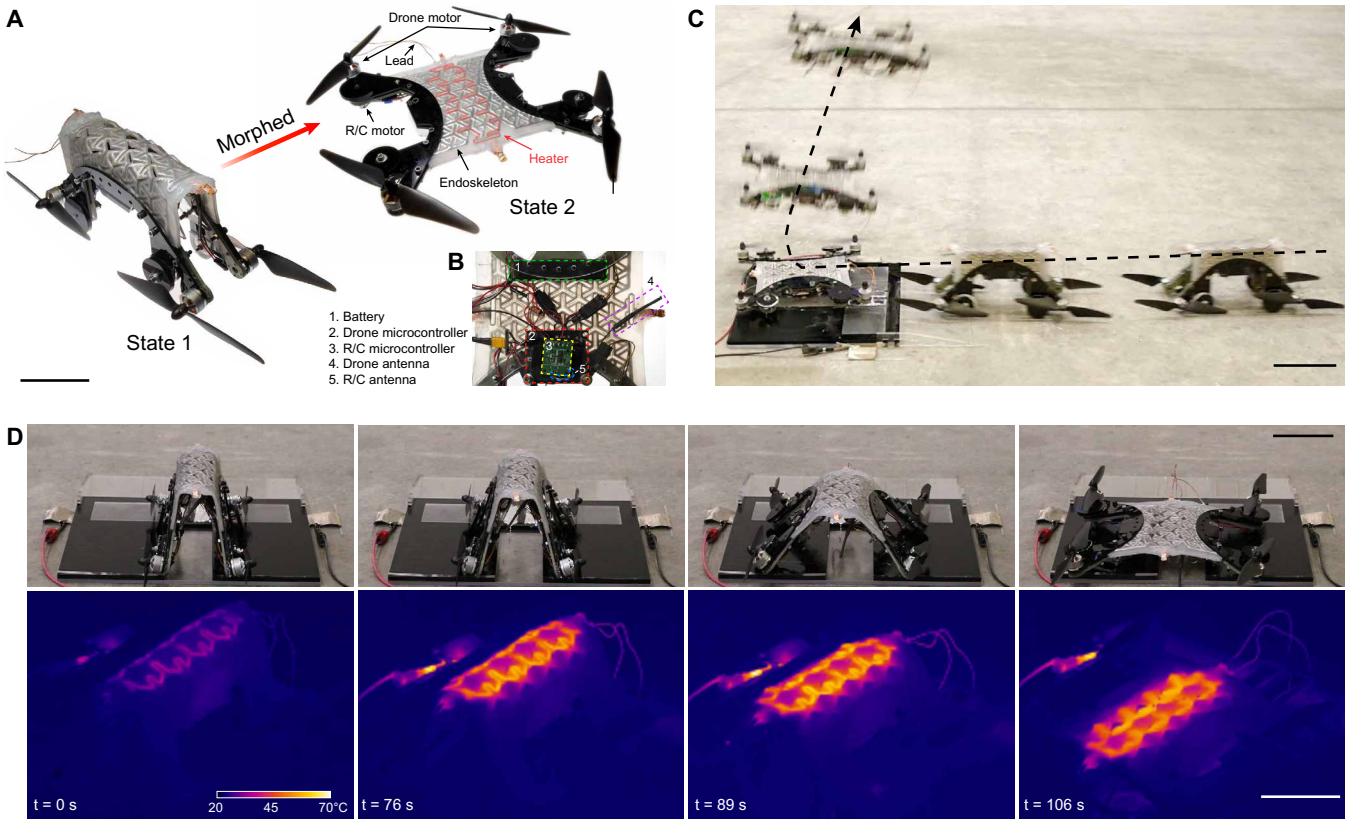

Fig. 4. Multifunctional autonomously morphing drone. (**A** and **B**) Photographs of the two distinct functional states of the soft robotic morphing drone and its integrated rigid electronics. State 1 is a land transport machine. State 2 is a fully functional quadrotor air vehicle. Scale bar, 60 mm. (**C**) Video frame sequence showing the morphing drone driving in state 1, transforming into the flying state, then taking flight in state 2 (movie S2). Scale bar, 100 mm. (**D**) Image sequence showing the transformation from states 1 to 2; the top row shows images, and the bottom row shows IR images. Scale bar, 60 mm.

transportable geometry (state 1), which is then sequentially morphed into a swimming state with features that interact with the environment to collect cargo (state 2), and then morph back to the retracted configuration (state 1) (Fig. 5A). The underwater machine consists of multiple stacked layers, including morphing kirigami composites with embedded liquid metal heaters, inflatable pneumatic membranes, and water propulsion channels. The pneumatic membranes on each side of the machine are individually controllable, which allows for independent morphing of the top and bottom layers and offers buoyancy control. Figure 5B illustrates the different states of the underwater machine. The machine was deployed by actuating the pneumatic membranes, which expanded to morph the composite layers. The morphed kirigami composites instantaneously became fixed into the deformed shapes and maintained their desired structure after the pneumatic membranes were deflated without consuming power. Upon completion of its task, the machine can be reversed to its original retracted shape using the embedded liquid metal heaters. This underwater morphing machine was capable of reversible deployment by morphing between the retracted state and deployed state, moving by water jet propulsion with buoyancy control, and interacting with the environment with rigid functional structures to collect cargo (Fig. 5C).

The morphing layers are multifunctional, providing structural shape, buoyancy control, and protection of the soft pneumatic membrane and allowing for environmental interaction. The bottom layer is designed to morph to collect cargo, enabling the machine to collect materials during deployment, and the top layer morphs and controls buoyancy for locomotion. The functionality of the underwater machine is demonstrated in Fig. 5D and movie S3. The underwater machine was dropped into the water in Fig. 5D(i) and immediately morphed and deployed to simultaneously achieve flotation and its functional form factor in Fig. 5D(ii). The bottom membrane was then deflated, producing an empty cargo bay with size and shape controlled by the bottom morphing composite layer. Next, air was removed from the top membrane to reduce the buoyancy of the underwater machine, causing it to descend. The water jets propelled the machine quickly toward the desired cargo at a speed greater than 210 mm s^{-1} (1.3 body lengths per second; movie S4). The machine then collected spherical, hydrogel beads as cargo. The top membrane was inflated, and the machine resurfaced by propelling forward in Fig. 5D(iii). The underwater machine was then retrieved in Fig. 5D(iv), and its cargo was emptied (Fig. 5E). Last, the machine was connected to an electrical power source, supplying power of 1.9 and 2.5 mW/mm^2 to the top and bottom heaters, respectively, where it reversed to its original, easily transportable shape. This implementation highlights the reversible deployability of morphing kirigami sheets, providing a platform for underwater robots that can morph into different functional shapes while moving through water to perform tasks such as sampling and transporting cargo.

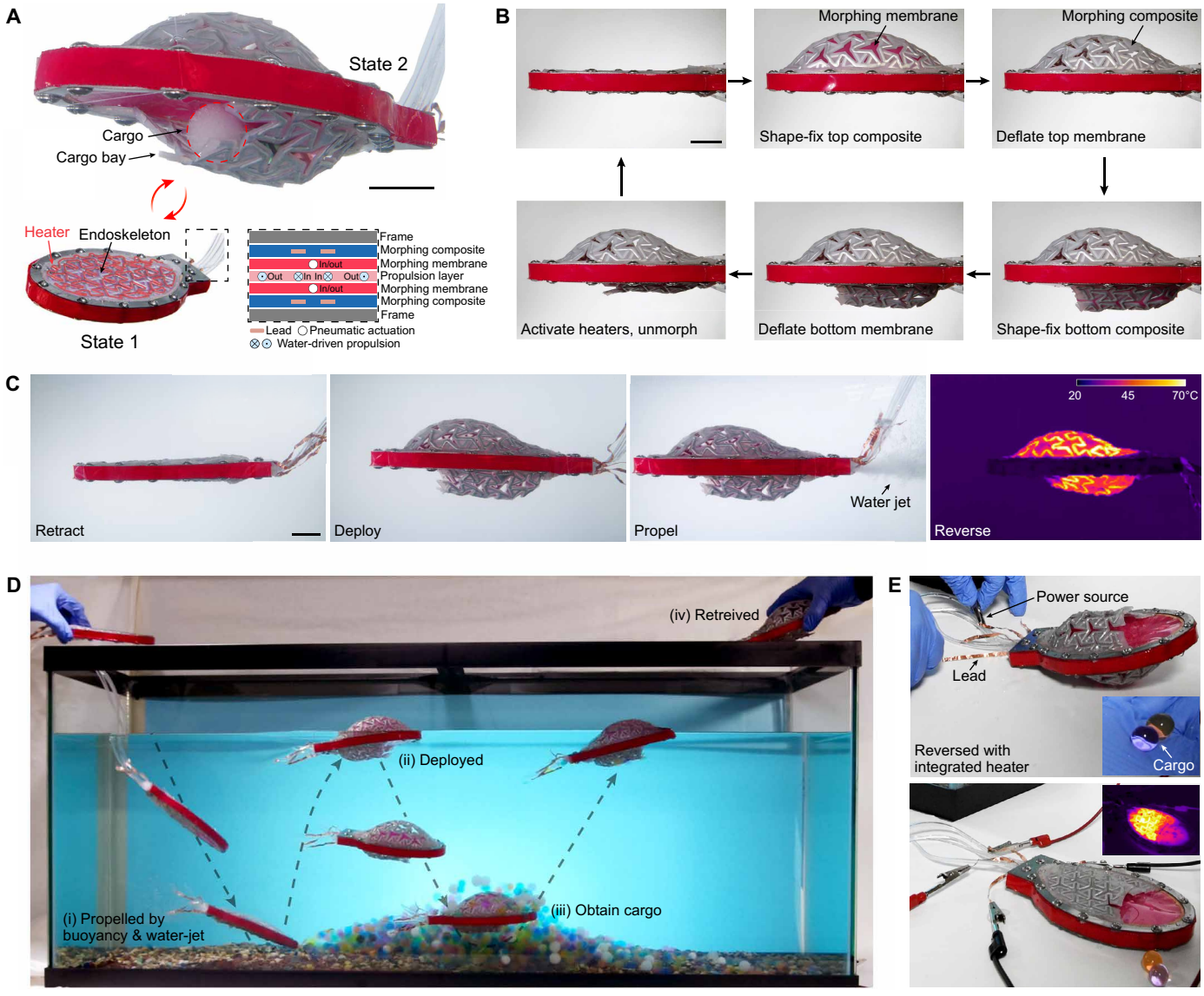

Fig. 5. Morphing and deployable underwater machine. (**A**) Photographs of the distinct functional states of the underwater morphing machine with a schematic showing the machine cross section. State 1 is a compact, retracted configuration for storage. State 2 is a functional deployed machine for underwater locomotion and cargo collection. Scale bar, 20 mm. (**B**) Image sequence showing the independent morphing, shape fixing, and reversibility of the top and bottom sides on the machine. (**C**) Images showing multifunctionality of the machine, which can deploy through instantaneous shape morphing and fixing, propel through water jetting, and reverse to a retracted state through integrated heaters. Scale bar, 20 mm. (**D**) Demonstration of the multifunctional underwater morphing robot that was deployed, locomoted through water propulsion and buoyancy control, obtained cargo, and retrieved (tubing is cropped out for clarity beyond the first image). (**E**) After retrieval, the cargo was emptied, and the machine was connected to a power source to activate reversibility to return to the original retracted state.

DISCUSSION

We have introduced a composite material system that can morph into diverse 3D shapes through kirigami-inspired structures, become instantaneously load-bearing through plastic deformation of the LMPA endoskeleton, and recover the initial shape through an unconventional reversible plasticity mechanism driven by the thermally induced phase transition of the LMPA. The combination of material plasticity and structural deformation provides a platform to simultaneously achieve reversible morphing and shape-fixing mechanisms at rapid time scales. Although plasticity is typically associated with permanent, irrecoverable deformation, by using LMPA we can induce plasticity and then "elastically" recover the deformation to reverse the plasticity. This recovery is achieved by activating the heaters, which causes the LMPA endoskeleton to melt, allowing the kirigami elastomer to both encapsulate the liquid and also elastically recover and guide the system back to the undeformed state. When the endoskeleton resolidifies, morphing can be performed again and a different shape can be achieved, where this reconfiguration process can be repeated over multiple cycles. Therefore, plasticity or deformation while the endoskeleton is in the solid state can be thought to switch on the shape shifting, and melting the endoskeleton with elastic recovery driven by the elastomeric

kirigami can switch off the shape shifting. If the endoskeleton fractures, the composite can also self-heal by melting the LMPA to repair the broken endoskeleton. Because the LMPA endoskeleton is embedded in kirigami-inspired architectures, large deformations can be achieved with high degrees of shape fixity combined with the ability to conform to complex geometries defined by nonzero Gaussian curvatures. Although LMPA fibers/sheets and kirigami approaches have been independently demonstrated, by introducing an LMPA endoskeleton embedded into kirigami structures, our integrated composite enables unique possibilities for advanced morphing systems. Our composite introduces a reversible plasticity mechanism in LMPAs to leverage material nonlinearities (plasticity and phase change), combined with kirigami structures that leverage nonlinear mechanical response, which allows for unique force-displacement relationships for efficient morphing to large deformations. This allows us to synergistically combine material and structural nonlinearities to achieve unique functionality, such as rapid shape morphing into complex shapes, which are immediately load bearing. In addition, we show that our composite morphs reversibly and does not consume power to hold the reconfigured state. Together, this represents an enabling combination of properties for integrated morphing systems.

The reversible plasticity mechanism enables nearly instant load-bearing capacity and high rigidity even after large deformations. One of the limitations in our current approach is the necessity to couple the shape-morphing composites with external actuation mechanisms. For the case of the multifunctional morphing drone, we did not use external actuation but relied on gravity to morph the vehicle in one direction, where further reconfiguration after the initial morphing step currently requires manual intervention. In the morphing membrane in Fig. 1 and in the morphing and deployable underwater machine in Fig. 5, we coupled the morphing composite with integrated pneumatic actuators. This allows for controlled transitions between multiple stable states through the reversible plasticity mechanism without external intervention. Therefore, the incorporation of actuation schemes is key to cyclic morphing behavior. In addition to the pneumatic actuators that we have used, other actuation schemes offer intriguing opportunities for integration into the shape-morphing composites presented here. These can include using soft active materials like liquid crystal elastomer (LCE) actuators (*27*, *46*), artificial muscles like shape memory alloy wires or carbon nanotube fibers (*47*, *48*), or tendon-driven actuation with electromechanical motors (*49*). Materials like LCEs could replace the currently passive elastomer layer where the LCE could be programmed to deform to different shapes (*50*). Artificial muscles and pneumatic actuation can also be directly incorporated into the elastomer layer or as a supporting layer (*51*). Electromechanical motors could be deployed into supporting structures, as has been done in foldable drones (*52*), or could be leveraged with fiber-driven actuation throughout the film (*53*). These different actuation approaches will require co-design with the shape-morphing composites through geometric and material selections to ensure optimal shape morphing and performance.

Our kirigami composite sheet allows us to achieve complex curvatures across the entire sheet, without having to preprogram specific deformations. Instantaneous load bearing is achieved through plasticity or phase change to reconfigure into different complex shapes. Although bistable systems can display different load-bearing configurations, creating multiple stable states often requires preprogramming or tiling subunits together, which can increase complexity and result in a restricted set of achievable morphologies. The kirigami composite sheet does not need preprogramming to achieve diverse configurations, which can be an advantage for reconfigurable or multifunctional applications. Furthermore, the materials and processes to make the kirigami composite sheets can be adapted to other kirigami or origami metamaterial approaches and geometries, which we anticipate could open further possibilities for deployable, architectured, or mechanical logic applications.

The materials presented here enable complex reconfigurations, load-bearing, and incorporation of functional components—including controllers, motors, and batteries—that can lead to dynamic functionalities in robotic systems. Because the reconfigured state is maintained without continuous energy supply, mobile and deployable machines can be reconfigured in the field for multiple tasks that require load-bearing capability. Although complex shapes have been achieved, optimization of kirigami layouts with embedded reversible plasticity could potentially enhance load-bearing capabilities. This could allow for additional functionalities such as field reconfigurable materials to rapidly support injuries or multipurpose robotics for gripping, carrying, or delivering supplies.

MATERIALS AND METHODS

Endoskeleton fabrication

We fabricated kirigami endoskeletons made of LMPAs [Field's metal, 32.5 weight % (wt %) bismuth, 16.5 wt % tin, and 51 wt % indium; RotoMetals] through replica molding and vacuum-assisted injection of liquid metals. A replica mold of polydimethylsiloxane elastomer (Sylgard 184 with a 20:1 base-to-curing agent ratio; Dow Corning) with the kirigami pattern was cleaned with isopropyl alcohol to remove all residues and was brought into contact with clean glass. Liquid Field's metal was placed on an inlet of the replica mold and was placed under vacuum for ~15 min (for the fabrication of LMPA skeleton in the drone demonstration, the vacuum time extended to 3 hours because of its larger scale). When the vacuum was released, the atmospheric air pressure pushed the liquid metal into the microchannels. After the channels were completely filled, the sample was removed from the oven to cool, and the metal skeleton was removed.

Embedded heating layer fabrication

Polyethylene terephthalate (PET) films (E = 2.6 ± 0.1 GPa, t = 75, 125 μm, Grainger) were patterned using a laser machine (Epilog Laser Fusion M2, 75 W), and then copper tapes (3M Inc.) were attached to both ends of the heater. The prepared sample was spray-coated across the entire sheet with liquid metal [eutectic gallium-indium (EGaIn)] and then sealed inside elastomeric sheets during the composite fabrication process.

Composite fabrication

Kirigami composites were composed of LMPA endoskeletons, embedded heating layers, and encapsulating elastomers. For all composites presented here, stacks of single-sided adhesive layers (t of single layer = 160 μm, Blazer Orange Laser Mask, IKONICS Imaging) were used to pattern bulk materials and control the thickness of each layer. First, a thin Dragon Skin layer (Dragon Skin 00-30, Smooth-on) was formed on a substrate within a stack of mask layers (t = 320 μm) using a thin-film applicator (ZUA 2000, Zehntner) and

then cured at 80°C for 5 min. The liquid metal–coated side of the prepared heating layer was placed onto the cured Dragon Skin layer. Another stack of mask layers (t = 480 μm) was attached, and a batch of Dragon Skin was formed within the frame (cured at 80°C for 5 min). The substrate was then cooled, and an LMPA endoskeleton was placed on the substrate in alignment with the heating layer underneath (cured at 80°C for 10 min). A last stack of mask layers (t = 960 μm) was attached, and the top Dragon Skin layer was formed (cured at 80°C for 10 min). The fabricated composite was then laser-machined to create kirigami films. To pressurize the LMPA endoskeleton channels, we placed the patterned composite on a hot plate (80°C) and injected excess liquid-state LMPA into the channels. The inlet was sealed back with glue (Sil-Poxy, Smooth-On). Embedded heaters were pressurized with liquid metal EGaIn with a syringe and needle. After filling, the injected hole was sealed with Sil-Poxy and cured for 12 hours.

Mechanical testing

Tests were conducted under uniaxial loading on an Instron 5944 mechanical testing machine with a 50-kN load cell at a loading rate of 1 mm/s and at various unloading rates. All mechanical data were analyzed with custom MATLAB code to measure stiffness and plastic strain at each step of each cycle. Copper leads were connected to a DC power supply to provide current when melting LMPA skeleton.

Morphing drone

The soft robot body was a kirigami composite composed of a single LMPA endoskeleton located between two embedded heaters connected in series and encapsulated in an elastomer. Drone components were harvested from a quadrotor drone (Drocon Bugs 3). The body was outfitted with a fiberglass and acrylic frame for integration of rigid electronics and machinery. We placed 6-mm-thick acrylic wheels at the four inner protrusions of the frame. The 4.5-cm-diameter rear wheels were adhered to 200 rpm brushed motors (Greartisan DC 6V), and the 4-cm-diameter front wheels were attached to screws and allowed to freely rotate. The soft robot was powered by a lithium polymer battery (7.4 V 1000 mAh, Tenergy) connected in parallel to the drone and remote-controlled car (Jeypod 2.4 GHz Racing Car) microcontrollers. Two 17-cm-long 20 AWG copper wires were connected to either end of the embedded heaters to allow for contact with the power transfer station. At the supplied power input of 9.3 mW/mm^2, the morphing drone changed shape from states 1 to 2 in ~1 min and 30 s with an active transformation time of ~2 s. Power was then turned off, and the morphing drone was cooled at room temperature for ~7 min before the drone took flight.

Underwater machine fabrication

The kirigami composite for both upper and bottom layer was composed of an LMPA endoskeleton and a liquid metal heater, which was encapsulated by the elastomeric layer. A 1/16″ solid acrylic layer was adhered between the top and bottom pneumatic systems with Sil-Poxy adhesive (Smooth-On) to allow for independent control of the membranes. The top system was composed of a 7/64″-thick acrylic sheet with cut channels to allow for insertion of a 3/32″-outer-diameter pneumatic tube for inflation of the membrane. The 7/64″ acrylic sheet was adhered with Sil-Poxy to a 700-μm-thick Dragon Skin membrane. The bottom system was composed of a 3/16″ acrylic layer with cut channels to allow for a 3/32″ outer diameter pneumatic tube and two 5/32″ outer diameter water propulsion tubes. A 700-μm-thick Dragon Skin membrane was adhered to the acrylic layer. Thick PET sheets (125 μm) were added to both the top and bottom Dragon Skin membranes to control the inflated shape. Stainless steel frames (1/32″) were placed on the outside of the kirigami composites. The layers were bolted together with #6-32 stainless steel binding barrels and screws. Water propulsion was controlled by a diaphragm pump (Hooshing 12V 60W diaphragm water pump).

Mechanical and finite element analysis

The analytical calculations were performed by considering only the geometry and material properties of LMPA endoskeleton, because its modulus and thickness were substantially higher than the elastomeric encapsulation and embedded heating layer. The kirigami structure was simulated using nonlinear finite element program ABAQUS (SIMULIA, Providence, RI) in the framework of 3D coordinate system. The 3D deformable shell objects were modeled using four-node reduced integration shell element with enhanced hourglass control. The composite layout feature of ABAQUS was used to develop the five-layered rigidity tuning endoskeleton, where the solid LMPA and heating layer were defined using elastoplastic behavior of Field's metal and PET, respectively. The elastomeric kirigami encapsulation of this endoskeleton was modeled by a hyperelastic model. We used an elastic modulus of E = 4.0 GPa and yield stress of E = 30.0 MPa to capture the LMPA behavior. The stress-strain relation of the elastomer was calibrated using nonlinear Yeoh hyperelastic model (*54*) by fitting to a strain energy function

$$U = \sum_{j=1}^{3}\left[C_{j0}\,[\bar{I}_1 - 3]^j + \frac{1}{D_j}[J-1]^{2j}\right] \quad (3)$$

where $J = det\ (\mathbf{F})$, $\bar{I}_1 = J^{-\frac{2}{3}tr(\mathbf{F}^T\mathbf{F})}$, and $\mathbf{F}$ represent volumetric deformation, first invariant, and deformation gradient, respectively. The material coefficients C_{10} = 0.16 MPa, C_{20} = 0.002 MPa, C_{30} = 0, and $D_1 = D_2 = D_3 = 0$ were used to incorporate the elastomers in the FE model. The material calibration parameters of elastomer (Dragon Skin) were curve-fitted to simulate the experimental stress-strain relation (see fig. S8). All these materials and section definitions were incorporated into the FEA simulation to validate the experimental elastoplastic character shown in Fig. 2B. Furthermore, the study on geometric configuration of LMPA beam composition was also simulated for various combinations of lengths (l_{LMPA}) and widths (w_{LMPA}).

Statistical tests

The meaning of all error bars and how they were calculated is described within the captions of the figures in which they occur.

SUPPLEMENTARY MATERIALS

www.science.org/doi/10.1126/scirobotics.abg2171
Figs. S1 to S8
Movies S1 to S4

REFERENCES AND NOTES

1. D.-H. Kim, J. Song, W. M. Choi, H.-S. Kim, R.-H. Kim, Z. Liu, Y. Y. Huang, K.-C. Hwang, Y.-w. Zhang, J. A. Rogers, Materials and noncoplanar mesh designs for integrated circuits with linear elastic responses to extreme mechanical deformations. *Proc. Natl. Acad. Sci. U.S.A.* **105**, 18675–18680 (2008).
2. N. W. Bartlett, M. T. Tolley, J. T. B. Overvelde, J. C. Weaver, B. Mosadegh, K. Bertoldi, G. M. Whitesides, R. J. Wood, A 3D-printed, functionally graded soft robot powered by combustion. *Science* **349**, 161–165 (2015).

3. B. Mosadegh, P. Polygerinos, C. Keplinger, S. Wennstedt, R. F. Shepherd, U. Gupta, J. Shim, K. Bertoldi, C. J. Walsh, G. M. Whitesides, Pneumatic networks for soft robotics that actuate rapidly. *Adv. Funct. Mater.* **24**, 2163–2170 (2014).
4. A. Tonazzini, S. Mintchev, B. Schubert, B. Mazzolai, J. Shintake, D. Floreano, Variable stiffness fiber with self-healing capability. *Adv. Mater.* **28**, 10142–10148 (2016).
5. T. C. Shyu, P. F. Damasceno, P. M. Dodd, A. Lamoureux, L. Xu, M. Shlian, M. Shtein, S. C. Glotzer, N. A. Kotov, A kirigami approach to engineering elasticity in nanocomposites through patterned defects. *Nat. Mater.* **14**, 785–789 (2015).
6. E. Hawkes, B. An, N. M. Benbernou, H. Tanaka, S. Kim, E. D. Demaine, D. Rus, R. J. Wood, Programmable matter by folding. *Proc. Natl. Acad. Sci. U.S.A.* **107**, 12441–12445 (2010).
7. Z. Zhakypov, K. Mori, K. Hosoda, J. Paik, Designing minimal and scalable insect-inspired multi-locomotion millirobots. *Nature* **571**, 381–386 (2019).
8. E. T. Filipov, T. Tachi, G. H. Paulino, D. A. Weitz, Origami tubes assembled into stiff, yet reconfigurable structures and metamaterials. *Proc. Natl. Acad. Sci. U.S.A.* **112**, 12321–12326 (2015).
9. M. Konakovic, K. Crane, B. Deng, S. Bouaziz, D. Piker, M. Pauly, Beyond developable: Computational design and fabrication with auxetic materials. *ACM Trans. Graph.* **35**, 1–11 (2016).
10. D. G. Hwang, M. D. Bartlett, Tunable mechanical metamaterials through hybrid kirigami structures. *Sci. Rep.* **8**, 3378 (2018).
11. D. P. Holmes, Elasticity and stability of shape changing structures. *Curr. Opin. Colloid Interface Sci.* **40**, 118–137 (2018).
12. A. Rafsanjani, D. Pasini, Bistable auxetic mechanical metamaterials inspired by ancient geometric motifs. *Extreme Mech. Lett.* **9**, 291–296 (2016).
13. H. Yasuda, J. Yang, Reentrant origami-based metamaterials with negative poisson's ratio and bistability. *Phys. Rev. Lett.* **114**, 185502 (2015).
14. M. A. Dias, M. P. McCarron, D. Rayneau-Kirkhope, P. Z. Hanakata, D. K. Campbell, H. S. Park, D. P. Holmes, Kirigami actuators. *Soft Matter* **13**, 9087–9092 (2017).
15. A. Rafsanjani, Y. Zhang, B. Liu, S. M. Rubinstein, K. Bertoldi, Kirigami skins make a simple soft actuator crawl. *Sci. Robot.* **3**, eaar7555 (2018).
16. A. Sedal, A. H. Memar, T. Liu, Y. Menguc, N. Corson, Design of deployable soft robots through plastic deformation of kirigami structures. *IEEE Robot. Autom. Lett.* **5**, 2272–2279 (2020).
17. G. P. Choi, L. H. Dudte, L. Mahadevan, Programming shape using kirigami tessellations. *Nat. Mater.* **18**, 999–1004 (2019).
18. Z. Zhai, Y. Wang, H. Jiang, Origami-inspired, on-demand deployable and collapsible mechanical metamaterials with tunable stiffness. *Proc. Natl. Acad. Sci. U.S.A.* **115**, 2032–2037 (2018).
19. L. Wang, Y. Yang, Y. Chen, C. Majidi, F. Iida, E. Askounis, Q. Pei, Controllable and reversible tuning of material rigidity for robot applications. *Mater. Today* **21**, 563–576 (2018).
20. Z. S. Davidson, H. Shahsavan, A. Aghakhani, Y. Guo, L. Hines, Y. Xia, S. Yang, M. Sitti, Monolithic shape-programmable dielectric liquid crystal elastomer actuators. *Sci. Adv.* **5**, eaay0855 (2019).
21. A. Sydney Gladman, E. A. Matsumoto, R. G. Nuzzo, L. Mahadevan, J. A. Lewis, Biomimetic 4D printing. *Nat. Mater.* **15**, 413–418 (2016).
22. J. H. Pikul, S. Li, H. Bai, R. T. Hanlon, I. Cohen, R. F. Shepherd, Stretchable surfaces with programmable 3D texture morphing for synthetic camouflaging skins. *Science* **358**, 210–214 (2017).
23. J. Kim, J. A. Hanna, M. Byun, C. D. Santangelo, R. C. Hayward, Designing responsive buckled surfaces by halftone gel lithography. *Science* **335**, 1201–1205 (2012).
24. D. P. Holmes, M. Roché, T. Sinha, H. A. Stone, Bending and twisting of soft materials by non-homogenous swelling. *Soft Matter* **7**, 5188–5193 (2011).
25. E. Siéfert, E. Reyssat, J. Bico, B. Roman, Bio-inspired pneumatic shape-morphing elastomers. *Nat. Mater.* **18**, 24–28 (2019).
26. H. Aharoni, Y. Xia, X. Zhang, R. D. Kamien, S. Yang, Universal inverse design of surfaces with thin nematic elastomer sheets. *Proc. Natl. Acad. Sci. U.S.A.* **115**, 7206–7211 (2018).
27. Q. He, Z. Wang, Y. Wang, A. Minori, M. T. Tolley, S. Cai, Electrically controlled liquid crystal elastomer-based soft tubular actuator with multimodal actuation. *Sci. Adv.* **5**, eaax5746 (2019).
28. Y. Kim, H. Yuk, R. Zhao, S. A. Chester, X. Zhao, Printing ferromagnetic domains for untethered fast-transforming soft materials. *Nat. Lett.* **558**, 274–279 (2018).
29. I. M. Van Meerbeek, B. C. Mac Murray, J. W. Kim, S. S. Robinson, P. X. Zou, M. N. Silberstein, R. F. Shepherd, Morphing metal and elastomer bicontinuous foams for reversible stiffness, shape memory, and self-healing soft machines. *Adv. Mater.* **28**, 2801–2806 (2016).
30. K. Yu, Q. Ge, H. J. Qi, Reduced time as a unified parameter determining fixity and free recovery of shape memory polymers. *Nat. Commun.* **5**, 3066 (2014).
31. T. L. Buckner, M. C. Yuen, S. Y. Kim, R. Kramer-Bottiglio, Enhanced variable stiffness and variable stretchability enabled by phase-changing particulate additives. *Adv. Funct. Mater.* **29**, 1903368 (2019).
32. F. Deng, Q. K. Nguyen, P. Zhang, Multifunctional liquid metal lattice materials through hybrid design and manufacturing. *Addit. Manuf.* **33**, 101117 (2020).
33. D. Zappetti, S. H. Jeong, J. Shintake, D. Floreano, Phase changing materials-based variable-stiffness tensegrity structures. *Soft Robot.* **7**, 362–369 (2020).
34. Y. Hao, T. Wang, X. Fang, K. Yang, L. Mao, J. Guan, L. Wen, A variable stiffness soft robotic gripper with low-melting-point alloy. *Chinese Control Conf. CCC* , 6781–6786 (2017).
35. J. Shintake, B. Schubert, S. Rosset, H. Shea, D. Floreano, Variable stiffness actuator for soft robotics using dielectric elastomer and low-melting-point alloy. *2015 IEEE/RSJ Int. Conf. Intell. Robot. Syst.* 1097–1102 (2015).
36. Y. Yang, M. A. Dias, D. P. Holmes, Multistable kirigami for tunable architected materials. *Phys. Rev. Mater.* **2**, 110601 (2018).
37. Y. Li, T.-c. Su, B. Ouyang, Design and deployment analysis of subsea deployable structures, *27th Int. Ocean Polar Eng. Conf.*, ISOPE–I–17–216 (2017).
38. T. Paschal, J. Shintake, S. Mintchev, D. Floreano, Development of bio-inspired underwater robot with adaptive morphology capable of multiple swimming modes. *2017 IEEE/RSJ Int. Conf. Intell. Robot. Syst.* 4197–4202 (2017).
39. G. Picardi, H. Hauser, C. Laschi, M. Calisti, Morphologically induced stability on an underwater legged robot with a deformable body. *Int. J. Rob. Res.* **40**, 435–448 (2021).
40. F. Giorgio-Serchi, A. Arienti, C. Laschi, Underwater soft-bodied pulsed-jet thrusters: Actuator modeling and performance profiling. *Int. J. Rob. Res.* **35**, 1308–1329 (2016).
41. F. Giorgio-Serchi, A. Arienti, F. Corucci, M. Giorelli, C. Laschi, Hybrid parameter identification of a multi-modal underwater soft robot. *Bioinspir. Biomim.* **12**, 025007 (2017).
42. J. Shintake, H. Shea, D. Floreano, Biomimetic underwater robots based on dielectric elastomer actuators. *IEEE Int. Conf. Intell. Robot. Syst.* 4957–4962 (2016).
43. G. Li, X. Chen, F. Zhou, Y. Liang, Y. Xiao, X. Cao, Z. Zhang, M. Zhang, B. Wu, S. Yin, Y. Xu, H. Fan, Z. Chen, W. Song, W. Yang, B. Pan, J. Hou, W. Zou, S. He, X. Yang, G. Mao, Z. Jia, H. Zhou, T. Li, S. Qu, Z. Xu, Z. Huang, Y. Luo, T. Xie, J. Gu, S. Zhu, W. Yang, Self-powered soft robot in the Mariana Trench. *Nature* **591**, 66–71 (2021).
44. W. Wang, N. G. Kim, H. Rodrigue, S. H. Ahn, Modular assembly of soft deployable structures and robots. *Mater. Horizons* **4**, 367–376 (2017).
45. A. D. Marchese, C. D. Onal, D. Rus, Autonomous soft robotic fish capable of escape maneuvers using fluidic elastomer actuators. *Soft Robot.* **1**, 75–87 (2014).
46. Q. He, Z. Wang, Y. Wang, Z. Wang, C. Li, R. Annapooranan, J. Zeng, R. Chen, S. Cai, Electrospun liquid crystal elastomer microfiber actuator. *Sci. Robot.* **6**, eabi9704 (2021).
47. M. D. Bartlett, N. Kazem, M. J. Powell-Palm, X. Huang, W. Sun, J. A. Malen, C. Majidi, High thermal conductivity in soft elastomers with elongated liquid metal inclusions. *Proc. Natl. Acad. Sci. U.S.A.* **114**, 2143–2148 (2017).
48. H. Chu, X. Hu, Z. Wang, J. Mu, N. Li, X. Zhou, S. Fang, C. S. Haines, J. W. Park, S. Qin, N. Yuan, J. Xu, S. Tawfick, H. Kim, P. Conlin, M. Cho, K. Cho, J. Oh, S. Nielsen, K. A. Alberto, J. M. Razal, J. Foroughi, G. M. Spinks, S. J. Kim, J. Ding, J. Leng, R. H. Baughman, Unipolar stroke, electroosmotic pump carbon nanotube yarn muscles. *Science* **371**, 494–498 (2021).
49. F. Renda, M. Cianchetti, M. Giorelli, A. Arienti, C. Laschi, A 3D steady-state model of a tendon-driven continuum soft manipulator inspired by the octopus arm. *Bioinspir. Biomim.* **7**, 025006 (2012).
50. T. H. Ware, M. E. McConney, J. J. Wie, V. P. Tondiglia, T. J. White, Voxelated liquid crystal elastomers. *Science* **347**, 982–984 (2015).
51. E. J. Markvicka, M. D. Bartlett, X. Huang, C. Majidi, An autonomously electrically self-healing liquid metal–elastomer composite for robust soft-matter robotics and electronics. *Nat. Mater.* **17**, 618–624 (2018).
52. D. Falanga, K. Kleber, S. Mintchev, D. Floreano, D. Scaramuzza, The foldable drone: A morphing quadrotor that can squeeze and fly. *IEEE Robot. Autom. Lett.* **4**, 209–216 (2019).
53. B. Mazzolai, A. Mondini, F. Tramacere, G. Riccomi, A. Sadeghi, G. Giordano, E. Del Dottore, M. Scaccia, M. Zampato, S. Carminati, Octopus-inspired soft arm with suction cups for enhanced grasping tasks in confined environments. *Adv. Intell. Syst.* **1**, 1900041 (2019).
54. O. H. Yeoh, Some forms of the strain energy function for rubber. *Rubber Chem. Technol.* **66**, 754–771 (1993).
55. D. Hwang, E. J. Barron III, A. B. M. Tahidul Haque, M. D. Bartlett, Dataset for a kirigami composite metamaterial sheet (2022); https://doi.org/10.7294/18306044.

Acknowledgments: We thank S. T. Frey for assistance with sample fabrication. **Funding:** We acknowledge support through Defense Advanced Research Projects Agency Young Faculty Award (DARPA YFA) (D18AP00041). **Author contributions:** D.H., E.J.B., A.B.M.T.H., and M.D.B. designed research; D.H., E.J.B., and A.B.M.T.H. performed research; D.H., A.B.M.T.H., and M.D.B. analyzed data; D.H., E.J.B., A.B.M.T.H., and M.D.B. wrote the paper. **Competing interests:** The authors declare that they have no competing interests. **Data and materials availability:** All data needed to evaluate the conclusions in the paper are presented in the paper or the Supplementary Materials and are available at the Virginia Tech Data Repository (*55*).

Submitted 17 December 2020
Accepted 18 January 2022
Published 9 February 2022
10.1126/scirobotics.abg2171

Science Robotics

Shape morphing mechanical metamaterials through reversible plasticity

Dohgyu Hwang, Edward J. Barron, III, A. B. M. Tahidul Haque, and Michael D. Bartlett

Sci. Robot. **7** (63), eabg2171. DOI: 10.1126/scirobotics.abg2171

Science Robotics (ISSN 2470-9476) is published by the American Association for the Advancement of Science. 1200 New York Avenue NW, Washington, DC 20005. The title *Science Robotics* is a registered trademark of AAAS.